Since January 2020 Elsevier has created a COVID-19 resource centre with free information in English and Mandarin on the novel coronavirus COVID-19. The COVID-19 resource centre is hosted on Elsevier Connect, the company's public news and information website.

Elsevier hereby grants permission to make all its COVID-19-related research that is available on the COVID-19 resource centre - including this research content - immediately available in PubMed Central and other publicly funded repositories, such as the WHO COVID database with rights for unrestricted research re-use and analyses in any form or by any means with acknowledgement of the original source. These permissions are granted for free by Elsevier for as long as the COVID-19 resource centre remains active.

Talanta 240 (2022) 123211

Contents lists available at ScienceDirect

Talanta

journal homepage: www.elsevier.com/locate/talanta

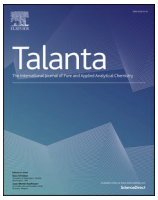

Electrochemical immunosensor for rapid and highly sensitive detection of SARS-CoV-2 antigen in the nasal sample

Mohammad Mehmandoust [a,b,*], Z. Pinar Gumus [c], Mustafa Soylak [d,e,f], Nevin Erk [a,b,**]

[a] Ankara University, Faculty of Pharmacy, Department of Analytical Chemistry, 06560, Ankara, Turkey
[b] Sakarya University, Biomaterials, Energy, Photocatalysis, Enzyme Technology, Nano & Advanced Materials, Additive Manufacturing, Environmental Applications, And Sustainability Research & Development Group (BIOENAMS R&D Group), 54187, Sakarya, Turkey
[c] Central Research Testing and Analysis Laboratory Research and Application Center, Ege University, Bornova, Izmir, 35100, Turkey
[d] Erciyes University, Faculty of Sciences, Department of Chemistry, 38039, Kayseri, Turkey
[e] Technology Research & Application Center (TAUM), Erciyes University, 38039, Kayseri, Turkey
[f] Turkish Academy of Sciences (TUBA), Cankaya, Ankara, Turkey

ARTICLE INFO

Keywords:
COVID-19
Spike protein
Metal-organic frameworks composite
Nasal sample

ABSTRACT

A label-free electrochemical biosensing approach as an appropriate analysis technique for SARS-CoV-2 spike protein (SARS-CoV-2 S-protein) was investigated to facilitate the diagnosis of coronavirus in real samples. It is crucial to construct diagnostic features that can rapidly identify infected individuals to limit the spread of the virus and assign treatment choices. Therefore, a novel and selective method using SiO_2@UiO-66 and a label-free electrochemical immunoassay for rapidly detecting spike protein. The development of innovative approaches for direct viral detection employing simplified and ideally reagent-free assays is a pressing and difficult topic. The absence of speedy and effective ways to diagnose viral diseases especially SARS-CoV-2 on demand has worsened the issue of combating the COVID-19 pandemic. The developed electrode illustrated a wide dynamic range of 100.0 fg mL^{-1} to 10.0 ng mL^{-1} with low limit detection. Therefore, the as-fabricated electrochemical SARS-CoV-2 S-protein sensor suggests an appropriate perspective in the point-of-care system, within 5.0 min, in nasal samples with satisfactory recovery.

1. Introduction

The new coronavirus disease 2019 (COVID-19), generated by the SARS-CoV-2 virus, which was first seen in Wuhan, China, on December 1, 2019, was announced a pandemic by the World Health Organization (WHO) and caused the death of more than 2 million people. Today, although there is no known effective treatment for coronavirus, the late diagnosis of this viral disease causes involvement in some essential organs in the body, especially the lungs, and leads to severe vital problems. Therefore, the tools developed for the correct and early diagnosis of the disease are of great importance. Moreover, it is worth noting that even in the most exceptional care centers, there are still requirements for swift and accurate techniques to provide monitoring of COVID-19. In clinical laboratories, although the reverse transcriptase-polymerase chain reaction (RT-PCR) is the most utilized technique for detecting the SARS-CoV-2 virus, it has some limitations [1–3]. Even though it contains minimally invasive procedures and ensures social distancing while sampling, its false-negative rate may range up to 37%. Its result may be yielded up to one day, and the deep sampling can be uncomfortable for some people [4]. Thus, the researchers have been directed to engineer alternative powerful tools for point-of-care applications. Considering that access to PCR tests is fraught with challenges in many parts of the world and its drawbacks mentioned above, it aims to develop an alternative method for detecting SARS-CoV2. In this regard, this study has developed reliable but less costly and faster diagnostic tests that determine antigens specific for SARS-CoV-2 infection. The Food and Drug Administration (FDA)-approved S-protein-detection diagnostic procedures are designed to accurately identify SARS-CoV-2 proteins produced by replicating viruses in respiratory secretions. They have been expanded as both laboratory-based tests and rapid diagnostic tests for near-patient usage.

Furthermore, thanks to their scalability, high sensitivity, selectivity, swift response time, relatively lower costs, and ease of application, the

* Corresponding author. Ankara University, Faculty of Pharmacy, Department of Analytical Chemistry, 06560, Ankara, Turkey.
** Corresponding author. Ankara University, Faculty of Pharmacy, Department of Analytical Chemistry, 06560, Ankara, Turkey.
E-mail addresses: mehmandoust@ankara.edu.tr (M. Mehmandoust), erk@pharmacy.ankara.edu.tr (N. Erk).

https://doi.org/10.1016/j.talanta.2022.123211
Received 2 December 2021; Received in revised form 31 December 2021; Accepted 4 January 2022
Available online 5 January 2022
0039-9140/© 2022 Elsevier B.V. All rights reserved.

electrochemical immunosensors have lately garnered attention to be utilized as a viable diagnostic tool for COVID-19. These superior characteristics make these sensors key tools for precise biomarker monitoring and early detection of various diseases. Formerly, the electrochemical techniques were already used to recognize specific antibodies of several deadly viruses. Nevertheless, one of the most critical issues with electroanalytical methods is surface interference induced by biomolecule adsorption, limiting their potential application. One viable solution to address this problem is the design of an effective electrochemical immunosensor modified with specific nanomaterials or molecules.

Intercommunication within the receptor-binding domain of spike protein and the peptidase domain of angiotensin-converting enzyme 2 (ACE2) facilitates SARS-CoV-2 entrance into the host cells. ACE2, a critical metalloproteinase, is employed to mediate COVID-19 viral infection [5]. ACE2 has been discovered to be a functional receptor for the S-protein of the SARS-CoV, leading to illness and transmission regardless of its peptidase activity. In addition, ACE2 is involved in acute lung injury and other organ damage. When ACE2 is placed on the apical surface of SARS-CoV-2 cells, it causes tenfold infection in the human body. As a result, therapies and research and development studies that target ACE2 have sparked a lot of attention to prevent viral infection and reduce organ damage. Even though recently there has been the phenomenon toward designing COVID-19 serological assays that recognize immunological or viral proteins in blood samples from infected individuals, alternative methods have been investigated due to the low sensitivity of these tests and the requirement of at least two antibodies. Indeed, the electroanalytical determination of SARS-CoV-2 antibodies has been considered to be a viable alternative. As far as the authors know, this is the first study to determine SARS-CoV-2 S-protein using an immunosensor in nasal samples with a novel SiO_2@UiO-66 nanocomposite.

Metal-organic frameworks (MOFs) are highly ordered crystalline materials created using coordination bonds to bind metal-containing units with organic linkers [6]. UiO-66 (Universitetet i Oslo-66) is a Zirconium (IV) carboxylate MOF made up of inorganic Zr6-octahedra bounded to twelve terephthalates ligands, which offers a high surface area and porosity, excellent thermal conductivity, enrichment capability, and chemical stability [7]. Due to their affordable costs and superior electrocatalytic activity, transition metals-UiO-based nanostructure have recently been extensively studied for modifying electrochemical sensors [8–12]. However, the issue of UiO-66's low electrical conductivity should be addressed to expand the detection concentration range for the analyte and boost the sensor's adsorption capacity. Thus, incorporating SiO_2 nanoparticles into an UiO-based framework to expedite electron transport and increase conductivity appears to be a viable strategy. Moreover, thanks to its large number of active sites, it can be expected to boost electrochemical activity.

In the light of all the aforesaid information, this work, it was aimed to develop a highly sensitive, relatively low-cost electroimmunosensor to determine SARS-CoV-2 S-protein, a biomarker of COVID-19. In this regard, a SiO_2@UiO-66 core-shell nanocomposite was synthesized via the rapid solvothermal method and utilized for modifying the screen-printed carbon electrode (SPCE) surface by drop-casting its dispersion on the electrode surface for the sensitive and selective detection of SARS-CoV-2 S-protein. With this purpose, it was aimed to design an immunosensor based on a novel nanocomposite for label-free detection of SARS-CoV-2 S-protein modeled on attaching the coronavirus to the ACE2 surface which causes the virus to enter the organ. Hence, the electrode surface was modified using ACE2 to connect and interact with the SARS-CoV-2 S-protein. This MOF-based sensor was capable of directly analyzing the electrochemical interactions between the electrode-electrolyte interface of the sensor and viral protein. As a proof-of-concept application, a developed electrochemical immunosensor was employed as a sensing platform to determine SARS-CoV-2 S-protein in nasal samples. The results offered that the developed sensor could be utilized to detect COVID-19 in a quick, low-cost way with high sensitivity, suggesting it an effective alternative for point-of-care COVID-19 testing. The fabrication procedure and action mechanism of the immunosensor are shown in Scheme 1.

2. Materials and methods

2.1. Materials and apparatus

The antigen of SARS-CoV-2 (S-protein) and Fc-tag-tagged human ACE2 were acquired from Sino Biological (Beijing, China). Fc-tag-tagged human ACE2 was diluted using phosphate-buffered saline (PBS). Influenza-A (Flu-A) antigen was obtained from BiosPacific (CA, USA), whereas HCoV antigen (HK41 N) was obtained from Medix Biochemica (Finland). Moreover, Terephthalic acid, Zirconium (IV) chloride ($ZrCl_4$), tetraethyl orthosilicate (TEOS), cysteamine, glutaraldehyde, bovine serum albumin (BSA), L-ascorbic acid ($C_6H_8O_6$, 99.0%), L-cysteine ($C_3H_7NO_2S$, 97.0%), L-arginine ($C_6H_{14}N_4O_2$, 98.0%), dopamine hydrochloride ($C_8H_{12}ClNO_2$, 99%), L-glucose ($C_6H_{12}O_6$, 99.5%), uric acid ($C_5H_4N_4O_3$, 99.0%), potassium hexacyanoferrate (III) ($K_3Fe(CN)_6$, 99.5%), and potassium ferrocyanide (IIII) ($K_4Fe(CN)_6$, 99.5%) were purchased from Sigma Aldrich Co. (Germany). Zanamivir, Tenofovir, Ribavirin, Favipiravir, Remdesivir, Vitamin D were purchased from GlaxoSmithKline Pharm. San, Santa Farma Pharm. San, Sanovel Pharm, Abdi Ibrahim Co, Novagentek Lab, Deva. Pharm. were purchased, respectively. All materials are analytical or HPLC grade and used directly without any purification.

Various spectroscopic and microscopic approaches were used to characterize the synthesized UiO-66-based composites. Fourier transform infrared spectroscopy spectra were collected on a PerkinElmer Spectrum. X-ray diffraction patterns of the samples were recorded by BRUKER AXS D8 ADVANCE (Waltham, MA, USA). Scanning electron microscopy images were obtained by Thermo Scientific Apreo S at an operating voltage of 3.00 kV (Netherlands). Thermogravimetric analysis (TGA) was conducted by TA instruments (SDT Q 600, USA). Various electrochemical characterization techniques, including cyclic voltammetry (CV), differential pulse voltammetry (DPV), and electrochemical impedance spectroscopy (EIS), were performed on an AUTO LAB system with PGSTAT128 N electrochemical workstation (Metrohm Inc, Switzerland) using a screen-printed carbon electrode (Dropsens Inc.) system to investigate the electrochemical performance of fabricated electrochemical immunosenor.

2.2. Synthesis of SiO_2@UiO-66 nanocomposite

The composite was synthesized according to the previous works reported by Yan et al. Mahmood et al., and El-Mehalmey with some modifications [13–15]. In brief, 327.5 mg of terephthalic acid (327.5 mg) and 512.5 mg of $ZrCl_4$ (512.5 mg) were dispersed in 25.0 mL N, N-Dimethylformamide (DMF) and placed into a Teflon-lined bomb. Following by sealing tightly, it was kept in a vacuum oven at 120 °C for 24 h. After cooling to room temperature, it was centrifuged, and the collected product was rinsed many times with the DMF and ethyl alcohol solution. Subsequently, the obtained UiO-66 nanoparticles were dried in a vacuum oven at 150 °C overnight. Afterward, a post-synthetic surface modification of UiO-66 was performed. For this purpose, 100.0 mg of UiO-66 with 1.0 mL of tetraethyl orthosilicate (TEOS) were mixed and kept in a vacuum oven at 80 °C for over 3 h. Finally, the as-obtained SiO_2@UiO-66 nanostructure was washed with methanol three times and dried at 50 °C in a vacuum oven overnight.

2.3. Fabrication of electrochemical immunosensor

To fabricate the electrochemical immunosensor, 10.0 μl of an aqueous dispersion of SiO_2@UiO-66 nanocomposite, and 10.0 μl of cysteamine (5.0 mM) was incubated consecutively on the surface of the

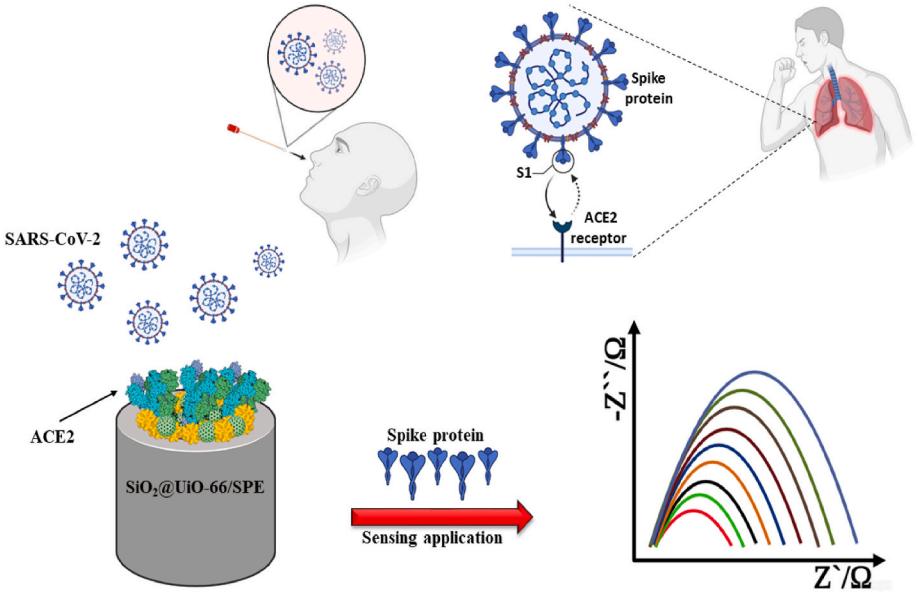

Scheme. 1. Schematic of the preparation and act mechanism of immunosensor.

SPCE at room temperature. After incubation, the modified electrode surface was washed with deionized (DI) water several times to eliminate any unattached cysteamine on the surface. Afterward, 20.0 μL of a 2.0% glutaraldehyde solution was incubated on the cysteamine-SiO_2@UiO-66 surface, followed by washing with PBS. Antibody immobilization was performed using 10.0 μl of antibody solution (ACE2, 10.0 μg mL^{-1}, diluted in PBS) on the electrode surface. The electrode was then washed using PBS to remove the unattached substance from the surface. Subsequently, the electrode surface was incubated using 10.0 μL of 1.0% bovine serum albumin prepared in PBS buffer to block the possible binding sites of glutaraldehyde on the electrode surface. After that, the immunosensor was washed with PBS before being used in S-protein detection experiments. After this step, the period of each material's contact with the electrode, as well as the concentration of the substances employed in the immunosensor fabrication, were investigated and optimized [16].

2.4. Optimization studies for increasing the electroanalytical activity of the immunosensor

The most important experimental conditions that can directly affect the immunosensing capabilities are the amount of modifier and antibody, incubation time, and pH. The optimized parameters for this work were tabulated in Table S1. The magnitude of response current decreases upon increasing the incubation time due to increased binding between spike protein and ACE2, indicating electron transfer resistance. A consistent response current was obtained after an incubation time of 5.0 min. This short response time may be related to the constant stirring (200 rpm) of the solution and the rapid binding between spike protein and ACE2. On the other hand, the large surface area of SiO_2@UiO-66 nanocomposite enhances the binding density of antibodies, and its high carrier mobility results in the capture of more target analytes, and also many cysteamine amino groups are enabled to gather considerable protein molecules. Therefore, this developed immunosensor significantly reduces the response time for S-protein identification. The impact of the ACE2 concentration captured on the electrode surface was investigated for the immunoassay. The current response enhanced distinctly as the increase of ACE2 level and arrived at a plateau after 10.0 μg mL^{-1}, and after that it remained almost unchanged with the further concentration of antibody increase, indicating the saturation of ACE2 on SiO_2@UiO-66/SPE. Therefore, 10.0 μg mL^{-1} was chosen as the optimal ACE2 concentration for fabricating the immunosensor. Moreover, the effect of pH on immunesensor response was studied in the various pH between 4.2 and 8.2. The electrochemical response of the immunosensor increased by increasing the pH value from 4.2 to 7.2. With the further increase of pH values, the DPV response of the immunesensor decreased rapidly. Therefore, pH 7.2 was chosen for further experiments, which was closest to the physiological condition. Finally, the optimization of the nanocomposite concentration was performed to improve the sensitivity of the developed immunosensor toward S-protein determination. The effect of nanocomposite concentration on the electrochemical response was measured in the concentration range of 0.1–2.0 mg mL^{-1} and increasing the SiO_2@UiO-66 concentration from 0.1 to 1.0 mg mL^{-1} enhanced the current percentage substantially. It may be due to a greater surface area and more adsorption functional sites are available. Moreover, at higher concentrations, there is a significant decrease, which might be related to aggregating accessible binding sites and decreasing the total available active surface area. Therefore, 1.0 mg mL^{-1} SiO_2@UiO-66 suspension was chosen as an optimum concentration.

2.5. Binding of SARS-CoV-2 S-protein onto the electrochemical immunosensor

The binding of SARS-CoV-2 S-protein onto the immunosensor was attained by adding 50.0 μL of SARS-CoV-2 S-protein solution over the SPE. Concentrations of SARS-CoV-2 S-protein in the range of 100.0 fg mL^{-1} to 10.0 ng mL^{-1} were prepared by sequentially diluting SARS-CoV-2 S-protein in PBS buffer and nasal fluid samples. Approximately 50.0 μL of each solution was incubated for 30 min to ensure binding with the immunosensor. Afterward, the immunosensor was washed in PBS before being used in the EIS analysis in the presence of $[Fe(CN)_6]^{3-/4-}$ as a redox probe.

3. Results and discussion

3.1. Physicochemical characterization of composite

The SiO_2@UiO-66 nanocomposites were characterized by several methods, including XRD, SEM, FTIR, EDX, and TGA. FT-IR spectra of the nanocomposite are depicted in Fig. S1. The characteristic peaks detected at 1058 and 810 cm^{-1} were ascribed to the stretching vibration of Si–O,

and the bending vibration of Si–*O*–H groups of the silica core, respectively [17,18]. The band at 1691 cm^{-1} was attributed to DMF [19], while the intense doublet observed at 1595 and 1410 cm^{-1} were associated with stretching modes of the carboxylate group [20]. In Zr–O peaks, at 746 and 630 cm^{-1} are assigned to longitudinal and transverse modes, respectively. Zr–O's peak position at 746 cm^{-1} is similar to the aromatic ring's C–H bending vibration [21,22].

Fig. S2 demonstrates the XRD pattern of the crystalline structure of SiO_2@UiO-66 nanocomposites. The XRD spectra of the SiO_2@UiO-66 exhibited a broad peak centered at *ca.*$2\theta = 25°$, showing an amorphous structure of SiO_2 [23]. Moreover, the peaks that appeared at *ca.*$2\theta = 7.1°$ and 8.55° were ascribed to the characteristic peaks of UiO-66. The excellent match between the XRD pattern of nanocomposite obtained in this work and the one published work in the literature confirmed that the production SiO_2@UiO-66 nanostructure was successfully achieved [24]. Furthermore, the weight-loss behavior of SiO_2@UiO-66 was investigated by TGA (Fig. S3). The TGA curve of nanocomposite was mainly divided into three steps: i) the evaporation of the surface water molecules at the temperature range of 80 and 120 °C, ii) the loss of solvent molecules trapped inside the micropores observed at a temperature ranging between 180 and 300 °C, and iii) a large amount of weight loss of SiO_2@UiO-66 detected at 480–570 °C, which was occurred during the decomposition of the organic linkers of UiO-66 (Fig. S3).

The surface morphology of the as-synthesized nanocomposite was investigated via SEM (Fig. 1A). The SEM images of the SiO_2@UiO-66 nanocomposite confirmes the formation of uniform dispersion with a regular spherical shape, with an average size of about 180 nm, revealing their nanoscale sizes. Furthermore, the SiO_2@UiO-66 nanocomposite was discovered to have a rough surface texture with obvious nanoparticles anchored on the spherical surface. Additionally, to determine the elemental composition of the nanocomposite, SEM-EDX spectra were obtained. The EDX spectra of the nanocomposite exhibited that the synthesized SiO_2@UiO-66 comprised only Si, Zr, C, N, and O elements, and there were no other remarkable impurities were detected (Fig. 1B).

3.2. Evaluation of electrochemical activity of the fabricated immunosensors for the determination of SARS-CoV-2

Evaluation of the electrochemical performance of the as-fabricated immunosensor was conducted in 5.0 mM $[Fe(CN)_6]^{3-/4-}$ containing 0.1 mM PBS with a pH of 7.2. The CV voltammograms of bare SPCE (BSPCE), SiO_2@UiO-66/SPCE, and BSA/ACE2/SiO_2@UiO-66/SPCE electrodes were depicted in Fig. 2A. As can be observed from Fig. 2A, after the modification of SPCE by the SiO_2@UiO-66, the value of the redox current of $[Fe(CN)_6]^{3-/4-}$ dramatically augmented as compared to the BSPCE. This was mainly attributed to the suitable electrochemical activity of SiO_2@UiO-66 accelerating the electron transfer on the electrode surface. It was realized that the redox current dropped drastically when ACE2 was immobilized on the modified electrode surface, and BSA was added as a blocker to avoid nonspecific binds. The immobilization of ACE2 reduced the peak current by confining the electron transfer between the electrode surface and the redox probe. In general, these decreases in current suggested that the immunocomplex formed successfully.

The EIS is an electrochemical analysis method that has widely been utilized to examine the electrochemical characteristics of the sensor surface [25]. Fig. 2B represented the Nyquist diagrams of developed immunosensor stepwise. The impedance of the BSPCE (curve b) was found to be relatively larger than that of the SiO_2@UiO-66/SPCE (curve a) (Fig. 2B). The surface resistance was considerably increased by effectively immobilizing ACE2 on the electrode surface (curve c of Fig. 2B) since the immobilized ACE2 hindered the electron transfer. As expected, by forming an immunocomplex between cysteamine, glutaraldehyde, and ACE2, the surface resistance and magnitude of electron-transfer resistance (R_{ct}) of the SiO_2@UiO-66/SPCE increased from 4.1 to 9.9 kΩ. After adding BSA (curve d) and SARS-CoV-2 S-protein (curve e), a low increase in the R_{ct} value was observed, indicating the successful immunocomplex formation between prepared surface and SARS-CoV-2 S-protein.

Chemical kinetics of SARS-CoV-2 S-protein on the electrode surface of SiO_2@UiO-66/SPCE was investigated by cyclic voltammetry technique in the presence of 5.0 mM $[Fe(CN)_6]^{3-/4-}$ containing 0.1 mM PBS at a pH value of 7.2, and different scan rates ranging between 10.0 and 300.0 mV s^{-1}. The plot of redox peak current *vs.* square root of scan rate was depicted in Fig. 3. The diffused-controlled behavior of the SiO_2@UiO-66/SPCE was demonstrated by its excellent linear behavior [26], indicating that this nanocomposite was qualified for SARS-CoV-2 S-protein detection.

3.3. Electrochemical determination of ACE2

The electrochemical response of the fabricated immunosensor towards various SARS-CoV-2 S-protein concentrations was shown in the Nyquist diagrams of Fig. 4A, and also the analytical plot obtained from Fig. 4A as illustrated in Fig. 4B. Within the wide concentration range of 100.0 fg mL^{-1} to10.0 ng mL^{-1}, a linear behavior was attained according to the equation of $\Delta R_{ct} = 6250 \log C\text{-}16607$ ($R^2 = 0.9917$). The concentrations of S-protein in the real samples were tested using this detection range as a reference. The detection limit (LOD) was chosen to be 100.0 fg mL^{-1} (detectable) for SARS-CoV-2 S-protein (concentrations

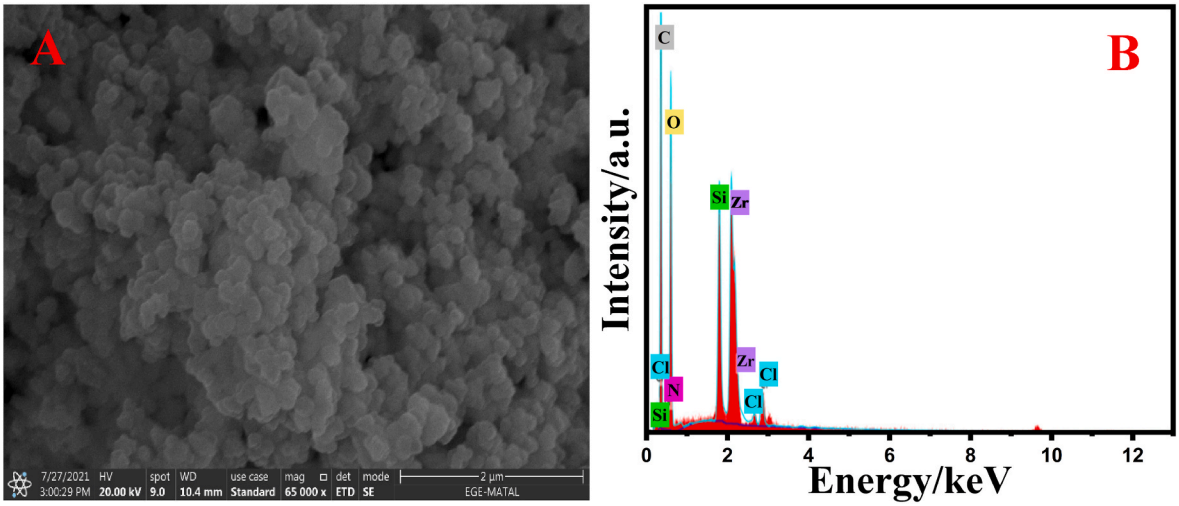

Fig. 1. (A); SEM image and (B); EDX of SiO_2@UiO-66 nanocomposite.

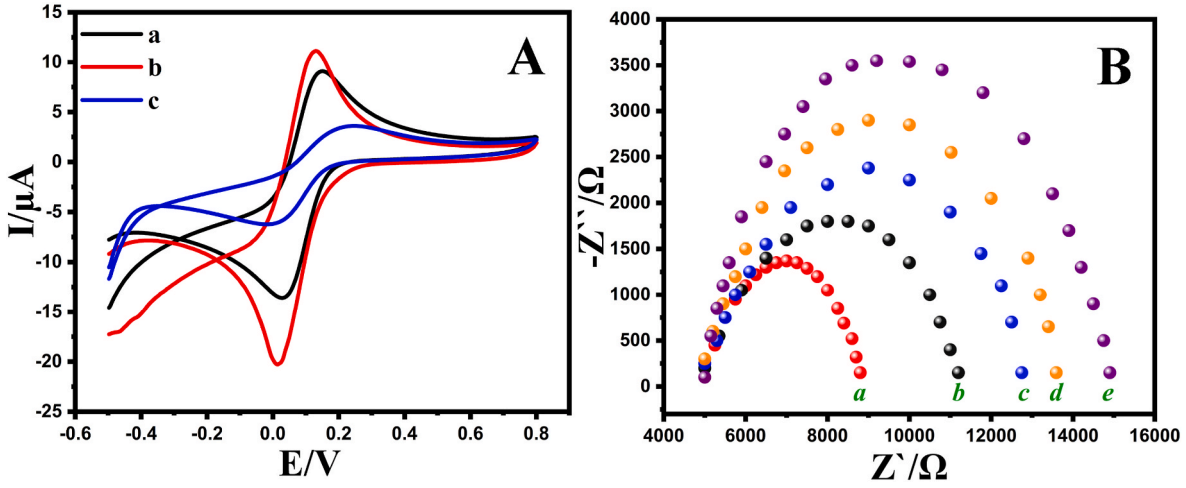

Fig. 2. (A) CV of BSPCE(a), SiO_2@UiO-66/SPCE (b), and BSA/ACE2/SiO_2@UiO-66/SPCE (c) and in a 0.1 mM PBS (pH 7.2) containing 5.0 mM $[Fe(CN)_6]^{3-/4-}$ at the scan rate 50.0 mVs^{-1}. (B) Nyquist plots obtained SiO_2@UiO-66/SPCE (a), BSPCE (b), ACE2/SiO_2@UiO-66/SPCE (c), BSA/ACE2/SiO_2@UiO-66/SPCE (d), and S-protein/BSA/ACE2/SiO_2@UiO-66/SPCE (e) in a 0.1 mM PBS (pH 7.2) containing 5.0 mM $[Fe(CN)_6]^{3-/4-}$.

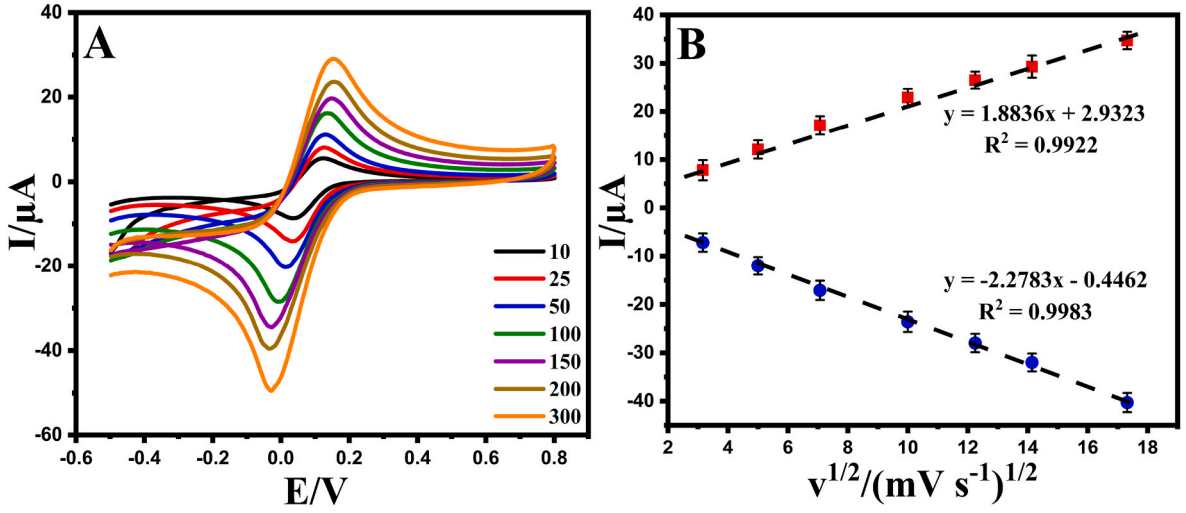

Fig. 3. (A); The cyclic voltammograms of 5.0 mM $[Fe(CN)_6]^{3-/4-}$ containing 0.1 mM PBS (pH 7.2) at SiO_2@UiO-66/SPCE at various scan rates 10.0–300.0 mV s^{-1}, (B); The plot of I_{pa} vs. $\nu^{1/2}$ relative to electrooxidation of 5.0 mM $[Fe(CN)_6]^{3-/4-}$ at SiO_2@UiO-66/SPCE.

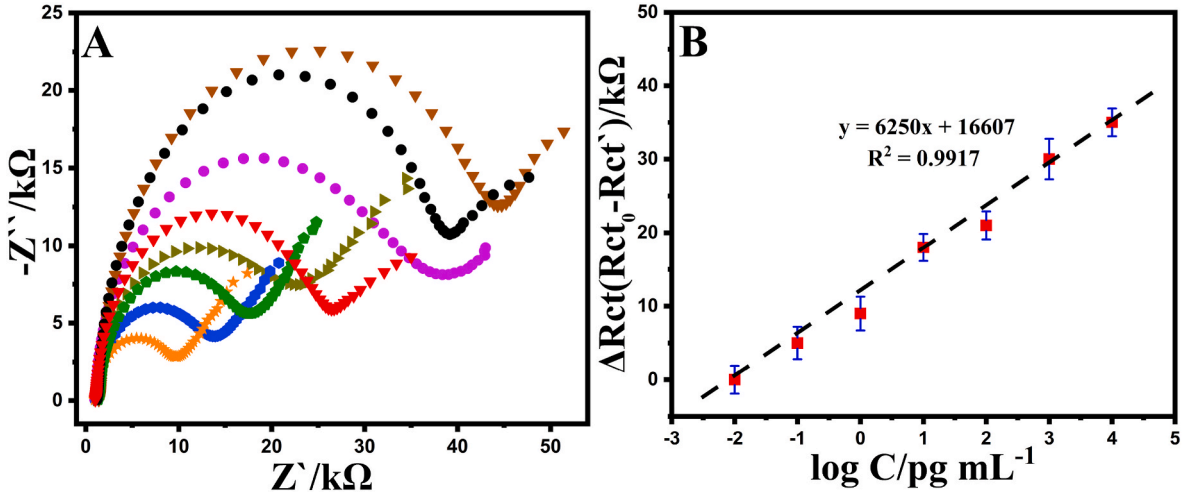

Fig. 4. (A); Nyquist plots obtained SiO_2@UiO-66/SPCE at various concentrations of SARS-CoV-2 protein S-protein, (B); The plot of logarithm concentrations against Δ Rct.

less than 100.0 fg mL $^{-1}$ do not cause a change in the semicircle), showing excellent sensitivity of the immunosensor.

Furthermore, Table 1 demonstrates several comparative approaches between the as-fabricated electrode to determine SARS-CoV-2 S-protein and the other techniques. The superiority of our work over previous research can be examined in four sections: (I) the low detection limit with low immunological response time (5.0 min), (II) high selectivity in nasal samples by this immunosensor, (III) low toxicity of the nanocomposite and reduced waste production, which indicates that it is environmentally friendly, (IV) no need for complicated preparation for developed sensor and real sample. Therefore, the as-fabricated electrode for the determination of SARS-CoV-2 S-protein could exhibit a potential for early COVID-19 detection.

3.4. Selectivity, reproducibility, and repeatability

The influence of the interfering agents on the electrochemical selectivity of the developed immunosensor was explored by a comparative analysis in the presence of interfering agents including Flu A (b), HCoV (c), L-glucose (d), L-cysteine (e), L-arginine (h), uric acid (n), dopamine (t), ascorbic acid (u), vitamin D (k), ribavirin (s), zanamivir (z), favipiravir (x), remdesiver (w), and tenofovir (m) by differential pulse voltammetry analysis. Fig. 5 illustrated the DPV voltammograms of the developed immunosensor in the presence of several interfering agents. Flu A (b), HCoV (c), L-glucose (d), L-cysteine (e), L-arginine (h), uric acid (n), dopamine (t), ascorbic acid (u), vitamin D (k), ribavirin (s), zanamivir (z) showed no or insignificant interference effect in the determination of SARS-CoV-2 S-protein. The calculated relative error values for SARS-CoV-2 S-protein were found to be less than 9%, which accords to the tolerance limit set in the selectivity measurements, suggesting that SiO2@UiO-66/SPCE provides superior selectivity for SARS-CoV-2 S-protein sensing.

A critical point worth noting in the electrode's selectivity was a notable reduction in current value, which could be due to the interaction between the favipiravir (x), remdesiver (w), and tenofovir with ACE2 receptors. This indicated the potent efficacy of these combinations for blocking the ACE2 receptor against SARS-CoV2. As a result, it may also be speculated that antiviral drugs like favipiravir, remdesiver, and tenofovir will lower coronavirus risk and successfully treat the disease. However, there is still need more scientific comprehensive works for the use of these drugs.

Moreover, the reproducibility and repeatability of the developed electrochemical immunosensors were investigated by EIS analysis (Fig. 6). Three identical electrodes modified under the same conditions were analyzed to assess the reproducibility of the immunosensor (Fig. 6A). The relative standard deviation (RSD) of the recorded current value was found as *ca.*4.85%, indicating good reproducibility of the immunosensor. Additionally, Fig. 6B represented the Nyquist diagrams of repeatability investigations, and the corresponding relative standard deviation value was calculated to be *ca.*6.64% for repeatability tests. Additionally, the reusability of developed was studied that showed the as-fabricated electrode is not disposable and can be used at least 10 times by only needs to be washed with hydrochloric acid (pH 2.0) and water to disrupt the binding between the ACE2 and S-protein after each analysis with 0.1 M PBS buffer [30].

Table 1
The comparison of developed electrodes with the other techniques.

Material	Linear range	LOD	Ref.
cobalt-functionalized TiO_2 nanotubes	14.0–1400 nmol L^{-1}	0.7 nmol L^{-1}	[27]
Paper-based electrochemical	1.0–1000.0 ng mL^{-1}	1.0 ng mL^{-1}	[28]
Carbon black-modified screen-printed	0.04–10 μg mL^{-1}	19.0 ng mL^{-1}	[29]
SiO_2@UiO-66/SPCE	100.0 fg mL^{-1} to 10.0 ng mL^{-1}	100.0 fg mL^{-1}	Our work

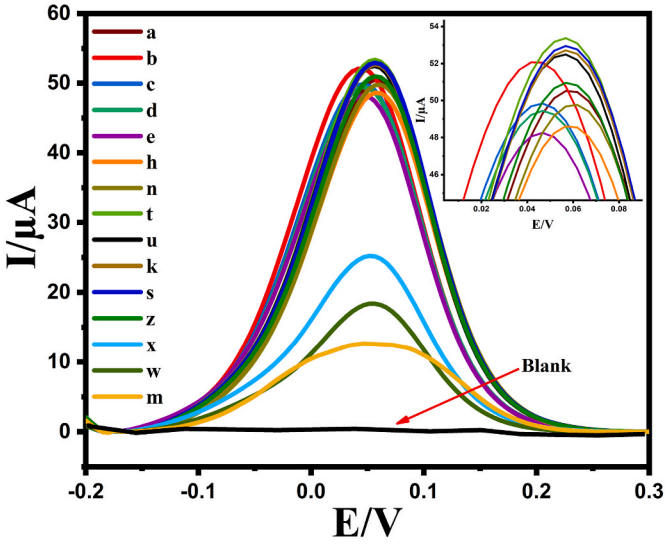

Fig. 5. DPV of SiO_2@UiO-66/SPCE in the presence of various interfering agents, including $[Fe(CN)_6]^{3-/4-}$ (a) Flu A (b), HCoV (c), L-glucose (d), L-cysteine (e), L-arginine (h), uric acid (n), dopamine (t), ascorbic acid (u), vitamin D (k), ribavirin (s), zanamivir (z), favipiravir (x), remdesiver (w), and tenofovir (m) in 10.0 mM $[Fe(CN)_6]^{3-/4-}$.

3.5. Detection of S-protein in real samples

The EIS approach was also employed to detect S-protein in nasal fluid samples to assess the reliability and accuracy of the label-free electrochemical immunosensor. The fabricated immunosensor determined the content of SARS-CoV-2 S-protein in the nasal sample according to the correlation between the current response and SARS-CoV-2 S-protein concentration ranging between 100.0 fg mL^{-1} to 10.0 ng mL^{-1}, in the presence of 5.0 mM $[Fe(CN)_6]^{-3/-4}$ (Fig. 7). The fabricated immunosensor measured the increase in impedance that corresponded to an increase in SARS-CoV-2 S-protein concentration. A linear relationship with an equation of $y = 5346.2x + 14{,}250$ ($R^2 = 0.954$) for the nasal sample was acquired. Moreover, the concentrations of 3000.0 fg mL^{-1}, 5000 fg mL^{-1}, and 4.0 ng mL^{-1} could be detected with satisfactory recovery values of 92.0, 91.6, and 93.2%, respectively, indicating the acceptable ability of the proposed sensor for the determination of SARS-CoV-2 S-protein in real samples. Furthermore, two samples in the presence and absence of antigen were examined in the nasal prepared solution and compared with the PCR test (COVID-19 Ag test, TÜRKLAB Co.). In the absence of antigene, no changes were observed using electrochemical immunosensor and PCR kit (only one line was observed), indicating an emphasis on the absence of the virus antigen in Covid tests. Finally, in the presence of antigene, PCR test and developed immunosensor showed the same results (positive), confirming the reliability of the developed immunosensor.

4. Conclusion

In this study, a novel, rapid, inexpensive, and ultraselective biosensor approach was studied for the determination of SARS-CoV-2 S-protein in nasal samples using an immunosensor based on SiO_2@UiO-66 nanocomposite. The developed immunosensor exhibited a low limit of detection of 100.0 fg mL^{-1} with minimal sample preparation steps, indicating the detection of SARS-CoV-2 S-protein was highly selective and reproducible with low response time (5.0 min total assay time). Moreover, the developed immunosensor could ultimately lead to more rapid clinical decision-making and corresponding determination in real samples.

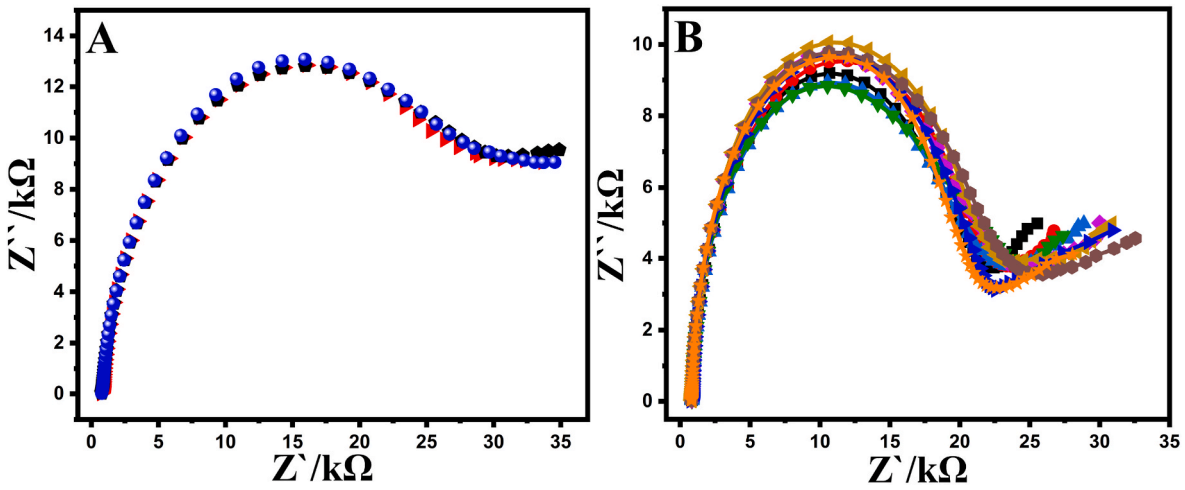

Fig. 6. Nyquist plots obtained SiO_2@UiO-66/SPCE at (A); reproducibility, (B); repeatability.

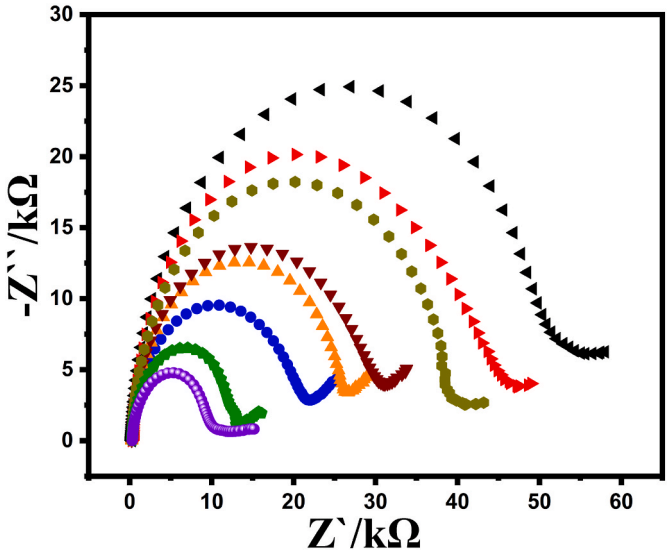

Fig. 7. Nyquist plots obtained SiO_2@UiO-66/SPCE at various concentrations of SARS-CoV-2 S-protein.

Credit author contribution statement

Mohammad Mehmandoust: Conceptualization, Methodology, Investigation, Validation, Data curation, Writing – original draft, preparation, Writing- Reviewing and editing draft preparation. **Nevin Erk**: Conceptualization, Methodology, Investigation, Validation, Data curation, Writing – original draft, preparation, Supervision, Resources. **Z. Pinar Gumus**: Methodology, Writing-Reviewing and editing draft preparation, Visualization. **Mustafa Soylak**: Conceptualization, Methodology, Writing – original draft, preparation, Writing- Reviewing and editing draft preparation.

Declaration of competing interest

The authors declare that they have no known competing financial interests or personal relationships that could have appeared to influence the work reported in this paper.

Acknowledgment

This work was supported by the Scientific Research Projects Commission of Ankara University (Project Number: 21B0237005and 21H0237005). Dr. M. Soylak is grateful for the financial support of the unit of the scientific research projects of Erciyes University (FYL-2021-11170) (Kayseri, Turkey). The authors gratefully acknowledge the TÜRKLAB company for providing PCR kits.

Appendix A. Supplementary data

Supplementary data to this article can be found online at https://doi.org/10.1016/j.talanta.2022.123211.

References

[1] D. Wang, B. Hu, C. Hu, F. Zhu, X. Liu, J. Zhang, B. Wang, H. Xiang, Z. Cheng, Y. Xiong, Clinical characteristics of 138 hospitalized patients with 2019 novel coronavirus–infected pneumonia in Wuhan, China, JAMA 323 (11) (2020) 1061–1069.

[2] T. Adelekan, B. Mihretu, W. Mapanga, S. Nqeketo, L. Chauke, Z. Dwane, L. Baldwin-Ragaven, Early effects of the COVID-19 pandemic on family planning utilisation and termination of pregnancy services in Gauteng, South Africa: march–April 2020, Wits J. Clinical Med. 2 (2) (2020) 145–152.

[3] Y. Tang, J.E. W Schmitz, D.H. Persing, C.W. Stratton, Laboratory diagnosis of COVID-19: current issues and challenges, J. Clin. Microbiol. 58 (6) (2020), 10.1128.

[4] S. Yang, R.E. Rothman, PCR-based diagnostics for infectious diseases: uses, limitations, and future applications in acute-care settings, Lancet Infect. Dis. 4 (6) (2004) 337–348.

[5] M.-Y. Liu, B. Zheng, Y. Zhang, J.-P. Li, Role and mechanism of angiotensin-converting enzyme 2 in acute lung injury in coronavirus disease 2019, Chronic diseases transl. med. 6 (2) (2020) 98–105.

[6] H. Furukawa, K.E. Cordova, M. O'Keeffe, O.M. Yaghi, The chemistry and applications of metal-organic frameworks, Science 341 (6149) (2013).

[7] Q. Yang, A.D. Wiersum, P.L. Llewellyn, V. Guillerm, C. Serre, G. Maurin, Functionalizing porous zirconium terephthalate UiO-66 (Zr) for natural gas upgrading: a computational exploration, Chem. Commun. 47 (34) (2011) 9603–9605.

[8] T. Zhang, J.-Z. Wei, X.-J. Sun, X.-J. Zhao, H.-l. Tang, H. Yan, F.-M. Zhang, Rapid synthesis of UiO-66 by means of electrochemical cathode method with electrochemical detection of 2, 4, 6-TCP, Inorg. Chem. Commun. 111 (2020) 107671.

[9] Q. Wang, X. Zhang, X. Chai, T. Wang, T. Cao, Y. Li, L. Zhang, F. Fan, Y. Fu, W. Qi, An electrochemical sensor for H2O2 based on Au nanoparticles embedded in UiO-66 metal–organic framework films, ACS Appl. Nano Mater. (2021), https://doi.org/10.1021/acsanm.1c00915.

[10] Z. Xu, L. Yang, C. Xu, Pt@ UiO-66 heterostructures for highly selective detection of hydrogen peroxide with an extended linear range, Anal. Chem. 87 (6) (2015) 3438–3444.

[11] L. Xu, J. Li, J. Zhang, J. Sun, T. Gan, Y. Liu, A disposable molecularly imprinted electrochemical sensor for the ultra-trace detection of the organophosphorus insecticide phosalone employing monodisperse Pt-doped UiO-66 for signal amplification, Analyst 145 (9) (2020) 3245–3256.

[12] M. Deng, S. Lin, X. Bo, L. Guo, Simultaneous and sensitive electrochemical detection of dihydroxybenzene isomers with UiO-66 metal-organic framework/mesoporous carbon, Talanta 174 (2017) 527–538.

[13] Z. Yan, J. Zheng, J. Chen, P. Tong, M. Lu, Z. Lin, L. Zhang, Preparation and evaluation of silica-UIO-66 composite as liquid chromatographic stationary phase for fast and efficient separation, J. Chromatogr. A 1366 (2014) 45–53.
[14] M.E. Mahmoud, M.F. Amira, S.M. Seleim, A.K. Mohamed, Amino-decorated magnetic metal-organic framework as a potential novel platform for selective removal of chromium (Vl), cadmium (II) and lead (II), J. Hazard Mater. 381 (2020) 120979.
[15] W.A. El-Mehalmey, A.H. Ibrahim, A.A. Abugable, M.H. Hassan, R.R. Haikal, S. G. Karakalos, O. Zaki, M.H. Alkordi, Metal–organic framework@ silica as a stationary phase sorbent for rapid and cost-effective removal of hexavalent chromium, J. Mater. Chem. 6 (6) (2018) 2742–2751.
[16] G. Wang, M.-L. Yang, Z.-L. Duan, F.-L. Liu, L. Jin, C.-B. Long, M. Zhang, X.-P. Tang, L. Xu, Y.-C. Li, Dalbavancin binds ACE2 to block its interaction with SARS-CoV-2 spike protein and is effective in inhibiting SARS-CoV-2 infection in animal models, Cell Res. 31 (1) (2021) 17–24.
[17] W. Li, Y. Xu, Y. Zhou, W. Ma, S. Wang, Y. Dai, Silica nanoparticles functionalized via click chemistry and ATRP for enrichment of Pb (II) ion, Nanoscale Res. Lett. 7 (1) (2012) 1–7.
[18] R. Mutneja, R. Singh, V. Kaur, J. Wagler, S. Fels, E. Kroke, Schiff base tailed silatranes for the fabrication of functionalized silica based magnetic nano-cores possessing active sites for the adsorption of copper ions, New J. Chem. 40 (2) (2016) 1640–1648.
[19] M. Nasrabadi, M.A. Ghasemzadeh, M.R.Z. Monfared, The preparation and characterization of UiO-66 metal–organic frameworks for the delivery of the drug ciprofloxacin and an evaluation of their antibacterial activities, New J. Chem. 43 (40) (2019) 16033–16040.
[20] L.J. Kirwan, P.D. Fawell, W. van Bronswijk, In situ FTIR-ATR examination of poly (acrylic acid) adsorbed onto hematite at low pH, Langmuir 19 (14) (2003) 5802–5807.
[21] J.H. Cavka, S. Jakobsen, U. Olsbye, N. Guillou, C. Lamberti, S. Bordiga, K. P. Lillerud, A new zirconium inorganic building brick forming metal organic frameworks with exceptional stability, J. Am. Chem. Soc. 130 (42) (2008) 13850–13851.
[22] R. Arrua, A. Peristyy, P. Nesterenko, A. Das, D. D'Alessandro, E. Hilder, UiO-66@ SiO 2 core–shell microparticles as stationary phases for the separation of small organic molecules, Analyst 142 (3) (2017) 517–524.
[23] W. Guo, S. Nie, E.N. Kalali, X. Wang, W. Wang, W. Cai, L. Song, Y. Hu, Construction of SiO2@ UiO-66 core–shell microarchitectures through covalent linkage as flame retardant and smoke suppressant for epoxy resins, Compos. B Eng. 176 (2019) 107261.
[24] X. Zhang, Q. Han, M. Ding, One-pot synthesis of UiO-66@ SiO 2 shell–core microspheres as stationary phase for high performance liquid chromatography, RSC Adv. 5 (2) (2015) 1043–1050.
[25] M. Mehmandoust, Y. Khoshnavaz, M. Tuzen, N. Erk, Voltammetric sensor based on bimetallic nanocomposite for determination of favipiravir as an antiviral drug, Microchim. Acta 188 (12) (2021) 1–15.
[26] M. Mehmandoust, S. Cakar, M. Ozacar, N. Erk, The Determination of Timolol Maleate Using Silver/Tannic acid/Titanium Oxide Nanocomposite as an Electrochemical Sensor in Real Samples, Electroanalysis.
[27] B.S. Vadlamani, T. Uppal, S.C. Verma, M. Misra, Functionalized TiO2 nanotube-based electrochemical biosensor for rapid detection of SARS-CoV-2, Sensors 20 (20) (2020) 5871.
[28] A. Yakoh, U. Pimpitak, S. Rengpipat, N. Hirankarn, O. Chailapakul, S. Chaiyo, Based electrochemical biosensor for diagnosing COVID-19: detection of SARS-CoV-2 antibodies and antigen, Biosens. Bioelectron. 176 (2021) 112912.
[29] L. Fabiani, M. Saroglia, G. Galatà, R. De Santis, S. Fillo, V. Luca, G. Faggioni, N. D'Amore, E. Regalbuto, P. Salvatori, Magnetic beads combined with carbon black-based screen-printed electrodes for COVID-19: a reliable and miniaturized electrochemical immunosensor for SARS-CoV-2 detection in saliva, Biosens. Bioelectron. 171 (2021) 112686.
[30] J. Choosang, S. Khumngern, P. Thavarungkul, P. Kanatharana, A. Numnuam, An ultrasensitive label-free electrochemical immunosensor based on 3D porous chitosan–graphene–ionic liquid–ferrocene nanocomposite cryogel decorated with gold nanoparticles for prostate-specific antigen, Talanta 224 (2021) 121787.